SUPPORTING INFORMATION

Terahertz-Driven Stark Spectroscopy of CdSe and CdSe:CdS Core:Shell Quantum Dots

Brandt C. Pein[*1], *Chee Kong Lee*[1], *Liang Shi*[1], *JiaoJian Shi*[1], *Wendi Chang*[1], *Harold Y. Hwang*[2], *Jennifer Scherer*[1], *Igor Coropceanu*[1], *Xiaoguang Zhao*[3], *Xin Zhang*[3], *Vladimir Bulović*[1], *Moungi Bawendi*[1], *Adam P. Willard*[1], *& Keith A. Nelson*[1]

**E-mail: bpein@mit.edu*

**Ph: 617-588-2128*

[1]Department of Chemistry and Department of Electrical Engineering and Computer Science, Massachusetts Institute of Technology, Cambridge, MA 02139 USA. [2]Massachusetts Institute of Technology Lincoln Laboratory, Lexington, MA 02420 USA. [3]Department of Mechanical Engineering, Boston University, Boston, MA 02215 USA.

Experimental apparatus

Vertically polarized terahertz (THz) pulses are generated in $LiNbO_3$ using tilted pulse front phase velocity matching[1], and are collimated onto an ITO-coated window using a pair of off-axis parabolic mirrors (Fig. S1a). The laser amplifier used to generate the THz pulses produces 4.5 mJ, 810 nm, 100 fs pulses. The time-dependent THz electric field was measured with electro-optic sampling[2,3] using a 100 μm thick 110-cut gallium phosphide crystal. At the focus, the maximum electric field of the THz pulses is 325 kV/cm with a frequency spectrum centered at 0.5 THz (Fig.

S1c). The peak THz electric field is adjusted using a pair of wire-grid polarizers. White light (WL) probe pulses with wavelength components spanning 450-700 nm (Fig. S1b) are generated by focusing laser amplifier pulses into a sapphire window and filtering the resulting emission through a 750 nm shortpass filter. The THz and WL pulses are spatially combined using the ITO-coated window and both are focused onto the sample using a third off-axis parabolic mirror. The THz spot at the sample is ~ 1 mm in diameter while the WL probe forms a 2-4 μm diameter spot size directed to a single microslit gap found within the THz spot area. The transmitted WL probe light is collected and imaged 1:1 on the spectrograph (Andor) slit using a pair of f/4 lenses. The spectrograph has an f/4 aperture, a 100 μm slit and 0.2 nm/pixel dispersion over a 1024x256 back-illuminated CCD camera.

Time-dependent Δσ spectra data workup

The white light probe pulse is positively chirped (longer wavelengths arrive first) so the probe wavelength components will arrive at the sample at different times during the probe pulse duration. As such, the Δσ spectrum will be distorted along the pump-probe delay axis and figure S2a and S2b illustrates this. Considering a simple pump pulse with a square temporal profile, as the pump-probe delay is increased the pump pulse is temporally overlapped with different wavelengths encompassing the probe spectrum. Assuming the pump pulse changes the absorption of the sample, this means for a fixed delay only those probe wavelengths temporally overlapped with the pump pulse will be absorbed by the sample. Continuing this logic for other delays and plotting the pump-probe data as a 2D surface a tilted time-dependent Δσ spectrum will result as in figure S2b.

To correct for the probe pulse chirp a shear mapping is applied to the data. The time-dependent Δσ data forms a 2D surface $\Delta\sigma(t,\lambda)$ for pump-probe delay t and probe wavelength λ. A suitable

shear mapping matrix M that translates each t,λ coordinate pair along the t axis a distance proportional to λ and can be written as

$$M = \begin{pmatrix} 1 & C \\ 0 & 1 \end{pmatrix}$$

where C is a constant and higher values of C produce more shear. Each t,λ pair in $\Delta\sigma(t,\lambda)$ is translated to a new position t',λ' by applying the shear matrix as such

$$\begin{pmatrix} t' \\ \lambda' \end{pmatrix} = \begin{pmatrix} 1 & C \\ 0 & 1 \end{pmatrix} \begin{pmatrix} t \\ \lambda \end{pmatrix}$$

Figure 2c shows an example of applying shear mapping to the data in sample I. Before mapping a slight tilt is shown in the raw Δσ data and after mapping the tilt is removed making the data more intuitive and easier to analyze.

QD synthesis

- Chemicals

1-octadecene (ODE, 90%), trioctylphosphine oxide (TOPO 99%), trioctylphosphine (TOP, 97%), oleylamine (OAm, 70%), 1-octanethiol (> 98.5%), sulphur powder (99.999%) were obtained from Sigma Aldrich. Cadmium oxide (CdO, 99.998%), selenium powder (99.999%), oleic acid (OLA, 90%) and octadecylphosphonic acid (ODPA, 97%) were purchased from Alfa Aesar.

- Synthesis of CdSe Cores

The synthesis of the CdSe cores and the first fast-injection shell growth were carried out by following a previously published procedure[4]. The first absorption feature of the cores was at 561 nm.

- Synthesis of the CdSe:CdS QDs

To a 250 mL round bottom flask was added 200 nmol of the CdSe cores (with a maximum of the first excitonic feature in the absorbance spectrum at 561 nm) dissolved in hexane, 5 mL of ODE, and 5 mL of oleylamine. The solution was degassed at r.t. for 2 hr. and then for 5 min at 100^{o}C to remove the hexane and water. The solution was then stirred under N_2 and the temperature was raised to 310^{o}C.

- Injection 1

At 200^{o}C, a solution of Cd-oleate (4 mL of a 0.2 M solution of Cd-oleate in ODE) dissolved in ODE and a separate solution of octanethiol (166 μL) dissolved in ODE (for a total volume of 10 mL each) were injected at a rate of 5.0 mL/hr. After the injection stopped after 2 hrs, an aliquot of 6 mL was taken after waiting for 5 additional minutes.

- Injection 2

Once the aliquot was removed, the same amount of precursors as used in injection 1 was added at a rate of 3.33 mL/hr. After the injection stopped after 1.5 hrs, a 10 mL aliquot was removed after waiting for 5 minutes. Oleic acid (2 mL) was then added.

- Injection 3

The same amount of precursors as used in injection 1 was again added at a rate of 3.33 mL/hr. After the injection ended after 1.5 hrs, the reaction was stopped by removing the heating mantle.

- Purification

Each aliquot was purified via precipitation of the particles using acetone followed by centrifugation at 5000 RPM for 5 min. The particles were then re-suspended in hexane.

QD size

Figure S3 shows TEM measurements of the QDs used in samples I and II. The CdSe cores used in sample I were measured to be 4.1 nm in diameter. The CdSe:CdS core:shell QDs in sample II have the additional 2.2-nm thick CdS shell.

Fabrication of the microslits

The microslits were fabricated using standard surface micromachining technique. A negative photoresist was spin coated on the SiO_2 substrate wafer, followed by UV exposure with a chrome mask and developing to define the microslit pattern. Then, a 15-nm-thick chrome adhesive layer and a 200-nm-thick gold layer were subsequently deposited on the wafer via electron beam evaporation. Finally, an acetone bath removed the remaining resist to form the microslit patterns.

Distribution of Electric Field Inside Microslit Gap

The time-dependent electric field inside a microslit gap was simulated using CST microwave studio[5].The field enhancement of a single gap at the peak of the time-dependent THz electric field is shown in figure S4a which is plotted along the *x,y* coordinates and is identical along the *z*-axis (parallel to the gap). The field enhancement forms an approximately parabolic shape along the *x*-axis (Fig. S4b) for each *y*-position (Fig. S4c). The probability distribution *P* of an electric field *i*, called P_i, can be described as

$$P_i = \frac{\Delta V_i}{\sum_i \Delta V_i} = \frac{\Delta V_i}{V}$$

where ΔV_i is the volume element of the microslit gap containing field *i,* the summation is performed over all field strengths within the gap, and *V* is the total volume within the gap. For both samples the probability distribution of the field was numerically computed from the simulated gap electric

field as shown in figure S5a where the field-axis is displayed in units of V/dot. First note that the probability distributions of both samples are identical in shape but, due to the different diameters of QDs found in these samples, the field-axis is linearly scaled by the QD diameter. Secondly, there are two peaks in both samples' electric field probability distribution. The first maximum near the lowest electric field values corresponds to regions near the middle of the gap, far away from the vertical Au walls where the field enhancement is strongest. The second peak at higher fields corresponds to regions near the vertical Au walls. The threshold electric field required to ionize the QDs via dot-to-dot charge separation is equal to the band gap energy $E_{band\text{-}gap}$ divided by QD diameter D

$$F_{thr} = \frac{E_{band-gap}(eV)}{D * e}$$

For samples I and II, F_{thr} is 2.2 and 2.0 V/dot respectively. Integrating the electric field probability distribution of both samples shows that none of the QDs in sample I experience charge separation while ~0.5% of the QDs in the sample II do. This is also evidenced by experimental THz-driven luminescence measurements shown in figure S5b. In our previous work[6] we demonstrated that QDs subject to fields $>F_{thr}$ luminesce due to dot-to-dot charge separation. Indeed it is clear that sample I shows no measurable luminescence in accordance with our simulations.

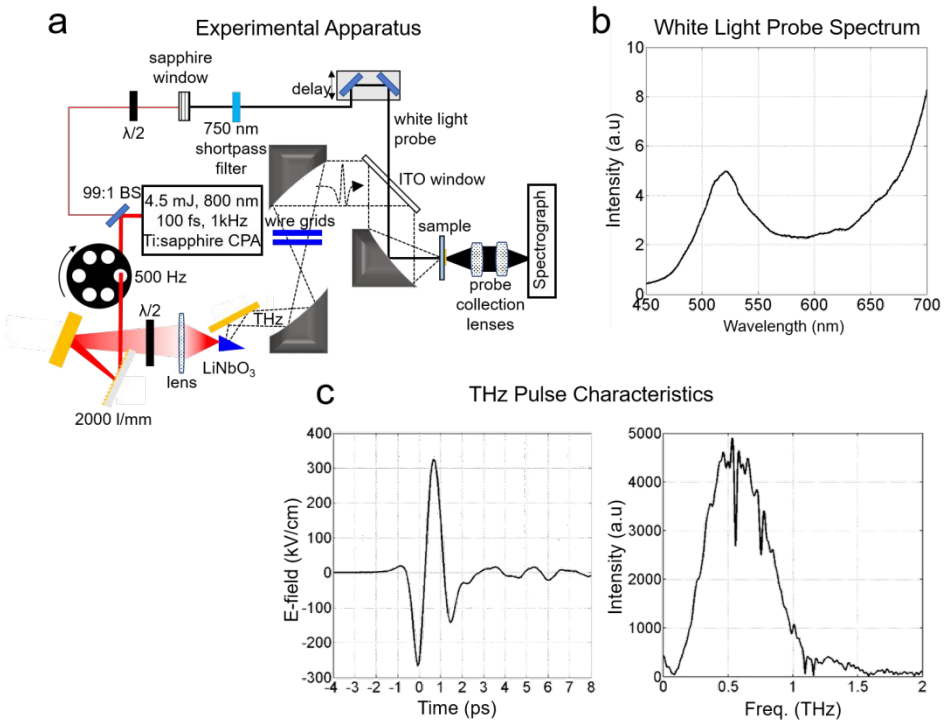

Figure S1 | Experimental apparatus and THz pulse characteristics. a, THz pulses are generated using the tilted pulse front phase velocity matching method and collimated using a pair of off-axis parabolic mirrors. White light probe pulses are generated in a 3-mm thick sapphire crystal, using a half-wave plate at adjust the optical pump intensity. The probe pulses are spatially combined with the collimated THz pulses using an ITO-coated quartz window. The THz and probe pulses are focused onto the microslit samples using a third off-axis parabolic mirror. The transmitted probe pulses are collected and measured using a spectrograph. **b,** The probe pulses are spectrally narrowed using a 750 nm shortpass filter resulting in wavelength components spanning 450-700 nm. **c,** The THz pulses have a maximum 325 kV/cm electric field and the spectrum of the THz pulses is centered at 0.5 THz. The sharp narrow dips in the THz spectrum are caused by water vapor in the air traversed by the THz pulses before reaching the sample.

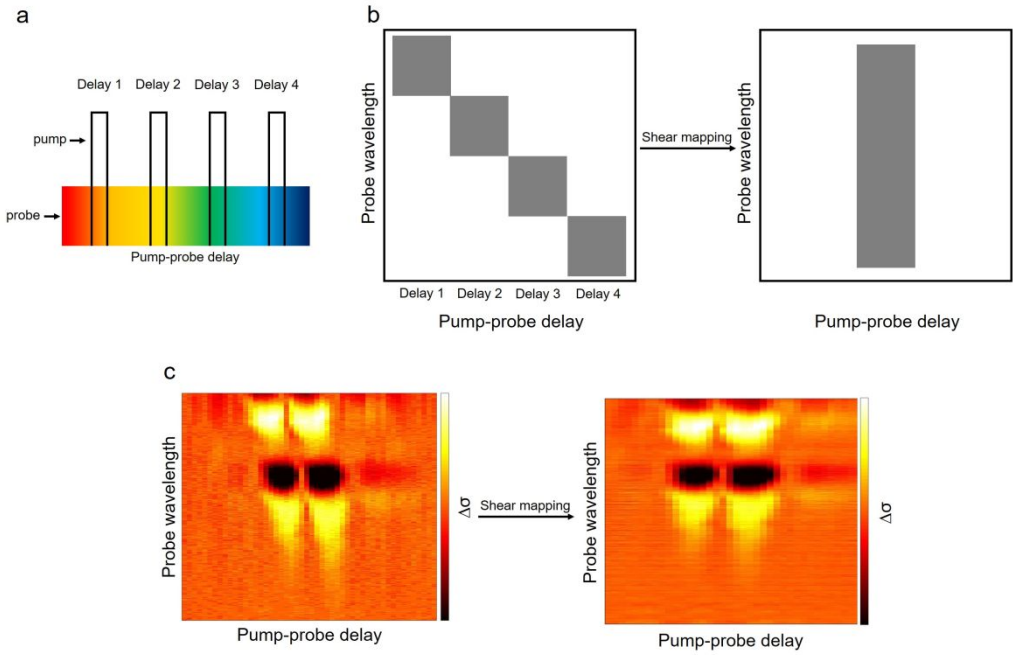

Figure S2 | Probe pulse chirp compensation. a, The white light probe pulses are chirped so different probe wavelengths will arrive at the sample and different pump probe delays. **b,** As such the Δσ spectra will be measured as a diagonal line (for a linear chirp). To compensate for the chirp, a shear matrix mapping is applied which shifts the pump-probe delay of each probe wavelength by a value proportional to the probe wavelength. **c,** As an example, the Δσ spectrum of sample I is shown before and after shear mapping is applied.

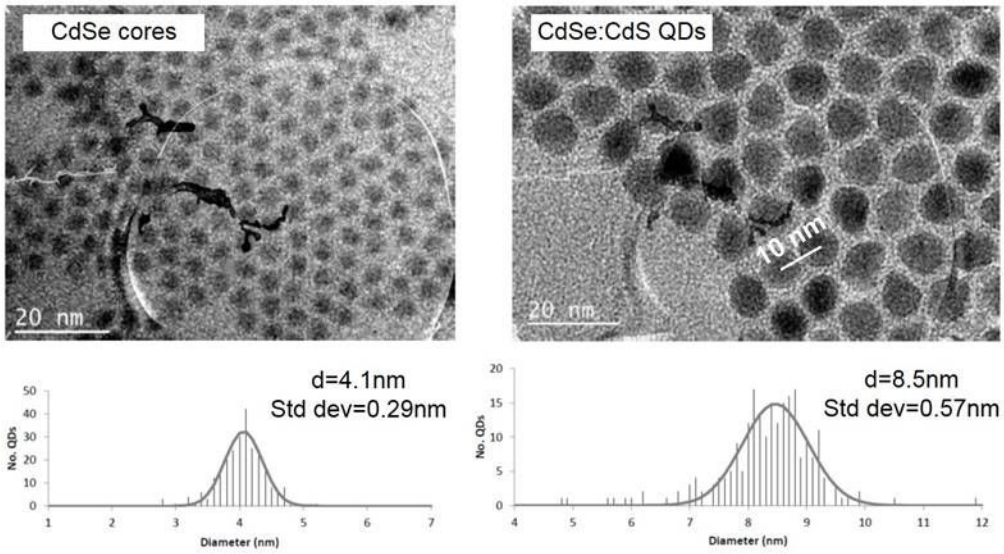

Figure S3 | SEM images of quantum dots. The CdSe cores have an average diameter of 4.1 nm. The addition of the CdS shell increases the average diameter to 8.5 nm, corresponding to a 2.2 nm thick shell.

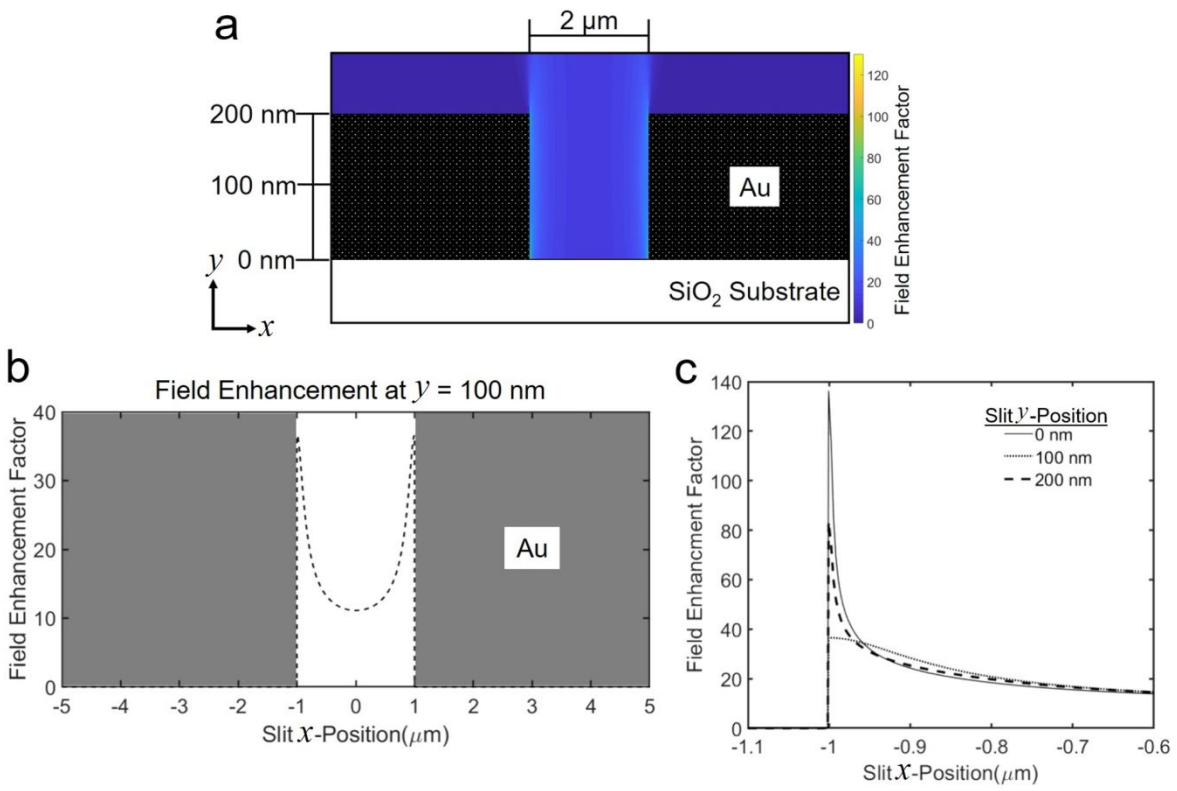

Figure S4 | Field enhancement simulation of microslit gap. a, The electric field enhancement with a microslit gap ranges between 10 and 140. The largest enhancement factors lie in regions nearest to the gold surfaces of the microslit (vertical components). **b,** The field enhancement, shown here at y=100 nm, has a roughly parabolic shape along the x-coordinate. **c,** The field enhancement has a similar shape for different y-positions (here shown nearest to the SiO_2 substrate, 100 nm, and 200 nm from the SiO_2 substrate) albeit with larger amplitude.

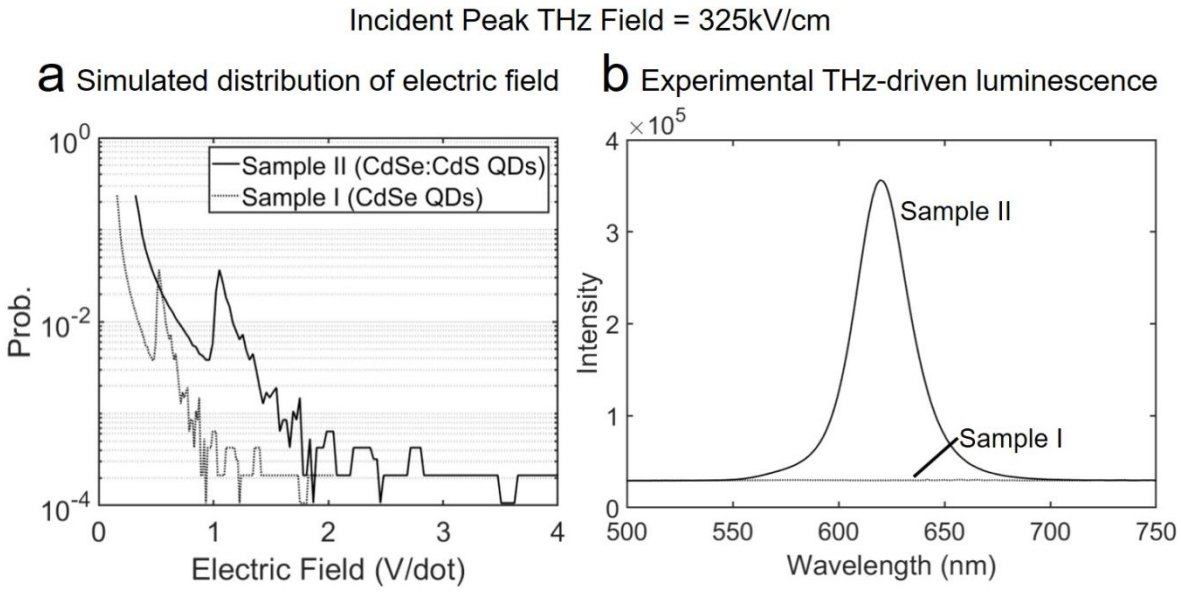

Figure S5 | Electric field distribution within a microslit gap for an incident THz peak field of 325 km/cm. a, The QDs in both samples see electric fields as high as 2-4 V/dot. Fields this high are capable of ionizing QDs via dot-to-dot charge separation. However, the vast majority of the QD layer experiences fields less than this. The threshold field (E_{thr}) for charge separation is 2.2 V/dot in sample I and 2.0 V/dot in sample II. Integrating the probability distribution of both samples from E_{thr} to infinity indicates that 0% of the QDs in sample I and 0.5% of the QDs in sample II experience fields above E_{thr}. **b,** To verify the field enhancement simulations, both samples were exposed to THz pulses with 325 kV/cm peak electric field (the maximum THz field used in this work). THz-driven luminescence is clearly observed in sample II while being absent it sample I. The absence of THz-driven luminescence in sample I is due to the smaller size of QDs; smaller QDs experience smaller electric fields (in units of V/dot).

References

(1) Yeh, K.-L.; Hoffmann, M. C.; Hebling, J.; Nelson, K. A. Generation of 10 MJ Ultrashort Terahertz Pulses by Optical Rectification. *Appl. Phys. Lett.* **2007**, *90* (17), 171121.

(2) Planken, P. C. M.; Nienhuys, H.-K.; Bakker, H. J.; Wenckebach, T. Measurement and Calculation of the Orientation Dependence of Terahertz Pulse Detection in ZnTe. *J. Opt. Soc. Am. B* **2001**, *18* (3), 313.

(3) van der Valk, N. C. J.; Wenckebach, T.; Planken, P. C. M. Full Mathematical Description of Electro-Optic Detection in Optically Isotropic Crystals. *J. Opt. Soc. Am. B* **2004**, *21* (3), 622.

(4) Carbone, L.; Nobile, C.; De Giorgi, M.; Sala, F. Della; Morello, G.; Pompa, P.; Hytch, M.; Snoeck, E.; Fiore, A.; Franchini, I. R.; et al. Synthesis and Micrometer-Scale Assembly of Colloidal CdSe/CdS Nanorods Prepared by a Seeded Growth Approach. *Nano Lett.* **2007**, *7* (10), 2942–2950.

(5) CST.com www.cst.com/products/cstmws.

(6) Pein, B. C.; Chang, W.; Hwang, H. Y.; Scherer, J.; Coropceanu, I.; Zhao, X.; Zhang, X.; Bulović, V.; Bawendi, M.; Nelson, K. A. Terahertz-Driven Luminescence and Colossal Stark Effect in CdSe-CdS Colloidal Quantum Dots. *Nano Lett.* **2017**.